Validation of Cable-Driven Experimental Setup to Assess Movements Made with Elbow Joint Assistance

Sreejan Alapati, Deep Seth, Sanjeevi Nakka, Yannick Aoustin

Journal Title
XX(X):1–12

DOI: 10.1177/ToBeAssigned
www.sagepub.com/
SAGE

Validation of cable-driven experimental setup to assess the efforts during elbow assistance

Sreejan Alapati[1,2] Deep Seth[1] Sanjeevi Nakka[1] and Yannick Aoustin[2]

Abstract

The article investigates the use of a cable-driven experimental setup to simulate the assistance in the sagittal plane provided by an exosuit to the elbow joint. Cable-driven exosuits, particularly fabric-based designs, can significantly enhance stroke rehabilitation by enabling targeted joint exercises and promoting functional recovery. These devices require an analysis of the cable tension, reaction forces, and moments, as well as their dependency on anchor points, to achieve an optimal design. This study presents a cable-driven experimental setup with two rigid bars and variable anchor points, designed to mimic the human forearm, upper arm, and elbow joint, to evaluate the performance of a potential cable-driven exosuit. Based on the experimental setup, a static model was developed to validate the measured cable tension and estimate the reaction force at the joint and the moments at the anchor positions. Furthermore, based on the observations, an optimization problem was defined to identify optimal anchor positions to improve the exosuit's design. Our findings suggest that prioritizing user comfort requires both anchor points to be as far away from the elbow joint as possible. However, for optimal exosuit performance, the forearm anchor position can be adjusted based on the joint angle while keeping the upper arm anchor position at the farthest point.

Keywords

Cable-driven exosuit, rehabilitation robot, exoskeleton, wearable and assistive devices, medical robotics

Introduction and Literature

Robotic assistance plays a crucial role in the rehabilitation of stroke patients [1,2], particularly by enabling the repetition of specific movements essential for recovery [2–5]. Numerous studies have demonstrated the benefits of using robotic devices to facilitate joint exercises [6], where repetitions are a key component of effective rehabilitation [5,7,8]. Among these technologies, cable-driven exosuits have gained attention for their ability to assist in repetitive tasks while allowing natural joint movement [9]. Fabric-based designs, in particular, offer simplicity and flexibility, making them well-suited for rehabilitation purposes [10].

Fabric-based cable-driven exosuits function by attaching anchor points to straps, which are then pulled by cables to induce movement [11,12]. This kind of exosuit actuation could be applicable to most joint motions, such as elbow joint, wrist, knee, ankle, etc [1] since its movement occurs primarily in a single plane. However, to optimize the performance of such devices, it is important to analyze key physical variables [13] such as cable tension, moments at the anchor points, and reaction forces. These factors vary depending on the load and the placement of the anchor points relative to the joint [14].

For the same load, these variables will change depending on the various distances of anchor points from the actuated joint. In other words, the design of the exosuit will affect these variables. For repetitive tasks, these forces may lead to wear and tear on the exosuit and subsequently reduce the performance of the device. These variables will also be important in designing with considerations for human safety and comfort [15].

Various models of exosuit actuation often assume a static approach [16,17]. For instance, CADEL [18] demonstrated the computation of string length and cable tension for fixed anchor points, while kinetostatic analyses of similar devices were also conducted in other studies [19–21]. However, they missed studying tensions and moments at various combinations of anchor point positions.

We focused the study on elbow joint because the literature reported studies on joint position during daily activities, focusing on elbow movement. Morrey et al. [22] examined tasks involving elbow flexion, while Oosterwijk et al. [23] analyzed various tasks requiring only elbow flexion, such as eating, typing, and using a doorknob. Although these tasks involve forearm rotation, the actuation of the elbow joint and forearm rotation is independent; thus, studies on either can be conducted separately. Since reaching is done by elbow flexion-extension, only elbow actuation is studied in this paper. Elbow flexion occurs in the sagittal plane, gravitational forces can be assumed to act within this plane when designing an exosuit.

In the proposed work, an experimental setup with a two-rigid-bar mechanism, which mimics the human arm with an elbow joint, has been developed to investigate the performance of a fabric-based cable-driven exosuit that can

[1]Department of Mechanical and Aerospace Engineering, Mahindra University, Hyderabad, India
[2]Nantes Université, École Centrale de Nantes, CNRS, LS2N, France

Corresponding author:
Deep Seth, Department of Mechanical and Aerospace Engineering, Mahindra University, Hyderabad, India
Email: Deep.Seth@mahindrauniversity.edu.in

be designed for elbow actuation in the future. Considering the low cost and strength, an experimentally tested[24] Nylon braided cable is used in the setup for joint actuation.

The study focuses on recording the tension in the cable and validating the results with a static model. In the context of rehabilitation, where device actuation occurs at low speed, the effects of inertial forces can be neglected. Thus, the current work predominantly considered a static model instead of a dynamic model to present force characteristics. The model assumes that the cable is always in tension and inelastic. This model is then used to assess the effects of reaction forces at the elbow and moments at the anchor points. The model assumes elbow flexion occurs in the sagittal plane, excluding any shoulder movement, which is also reflected in the experimental setup. Key inputs include the total weight supported by the exosuit (including external load), forearm length, and the distances from the joint to the anchor points. The model calculates the required holding torque for various flexion angles, cable tension, and cable length, as well as reaction forces at the elbow joint and moments at the anchor points caused by cable tension. Studies on bearable limb compression pressures and forces[25–27] help ensure that the forces predicted by the model result in a comfortable exosuit design. Additionally, the calculated torque values can guide motor selection for the actuation mechanism, while the relationship between cable length and flexion angle informs motor control for precise elbow positioning.

Based on the results, the study also investigated optimal anchor point positions for various load, aiming to improve tension, reaction forces, moments, and human comfort. It is expected that optimized physical variables will also improve the overall efficiency and performance of the suit[28]. The research objectives are

- To validate the experimental cable tension with a mathematical model during cable-driven elbow actuation for different anchor point positions.
- To comprehend reaction forces experienced at the elbow joint and moments at the anchor point attachments with the observed tension values.
- To optimize the anchor point position from the elbow joint to achieve better performance and wearer's comfort.

Methodology

The primary goal of this research is to test an experimental setup that mimics a cable-driven exosuit for elbow joint actuation with various locations of anchor points relative to the joint. Several studies on the design of cable-driven elbow actuation systems focus on optimizing the cable routing for elbow actuation[29,30]. These studies aim to optimize the anchor point positions around the axis of the forearm and upper arm while keeping the anchor point distance from the elbow joint fixed. Wei et al., studied the human-machine interaction forces by varying cable tension and keeping the distance of the anchor point from the elbow fixed[31]. These studies do not consider the effect of the anchor point position with respect to the elbow joint. Studying the effect of the distance of the anchor point from the elbow joint on a simple mechanism rather than having multiple cables around the axis of the upper arm and forearm, highlights the effect of the anchor of point position explicitly. This allows for understanding the importance of anchor point position from the elbow joint during the elbow actuation. The focus is on determining cable tension, perceived reaction forces at the joint, and moments at the anchor points. Through the development of an experimental setup, this work aims to address existing gaps in the literature related to anchor point positioning and its influence on the performance of the exosuit. By employing a static model and a practical experiment, this study will test the forces and moments associated with various joint angles. Further, the research also investigated determining the optimal anchor point configurations to enhance human comfort, design, safety, and the overall efficiency of the exosuit, making it suitable for rehabilitation applications in the future.

Experimental setup

The experimental setup was developed at Mahindra University to mimic the elbow joint assistance of the human arm using a cable-driven exosuit. The experimental setup replicates the movements of the upper and lower arm, allowing for the attachment of weights at the end to simulate different loads.

Structure The experimental setup, illustrated in Fig. 1, consists of aluminium profile rigid bars designed to mimic the human arm. One bar represents the upper arm and the other bar represents the forearm, both of length 0.3 m and weight 0.135 kg. The bars are connected by a hinge that simulates the elbow joint, allowing for approximate frictionless movement. The upper bar is fixed to the frame using a nut and bolt and can be adjusted at specific angles (but during the experiment, we keep the upper bar fixed vertically). The lower bar's angle can be adjusted in the range of 52° to 180°. Here, 180° represents the fully extended posture of the forearm. A hanging system has been designed to suspend the load at the end of the lower bar, to emulate different forearm weights as load.

To replicate the actuation mechanism of a cable-driven exosuit, a motor (Rhino RMCS 2103 DC motor) was mounted onto the aluminium profile bar, driving the braided nylon cable. The lower bar features an anchor point equipped with a load cell (50 kg capacity) to measure cable tension. This load cell is housed in a 3D-printed enclosure, which allows it to tilt so that the cable remains parallel to the measuring axis. The readings of the load cell can be viewed on an LCD display attached to the lower bar. A pulley, which acts as an anchor point, is positioned on the upper bar to guide the cable to the motor. The distance between the anchor points and the joint is adjustable to simulate different anchor positions. The motor was selected based on the static model calculations, presented in the section Static model, which estimated a required torque of 6 N·m to account for the weight of the forearm and hand (approximately 2 kg for an adult)[32]. A motor capable of handling a maximum load of 5 kg was chosen, incorporating a safety factor. The Arduino UNO microcontroller and joystick is used to actuate the motor to set the lower bar at the desired position. Overall,

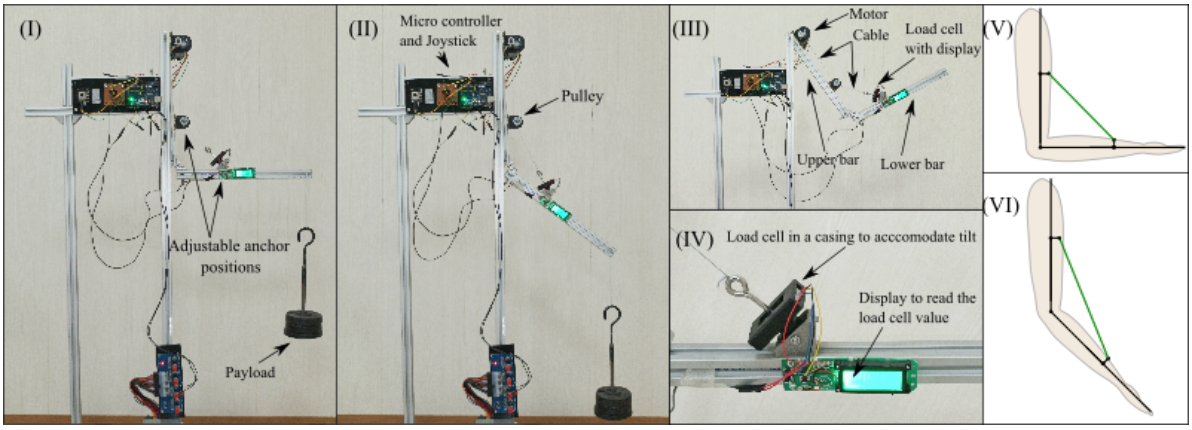

Figure 1. (I) and (II) show the experimental setup mimicking the human upper limb in two different joint positions, as represented in (V) and (VI). (III) and (IV) highlights the components of the experimental setup.

the experimental setup enables real-time monitoring of the cable tension for different joint angles and anchor positions.

Cable Selection In this experimental setup, for cable selection, we considered low cost, easy availability in the market, and durability as factors. Selecting the right cable for cable-assisted devices is essential for durability and reducing maintenance[24,33]. It is assumed that if cable performance is good in cyclic loading, then it should perform well in static loading for a similar load. Hence, a different experimental setup, as shown in Fig. 2a, is used to test cable resistance and wear under cyclic loading. A motor-driven pulley system is used to move weights up and down linearly at 0.025 m/s for a distance of 0.15 m. $V(t)$ is the ramp signal of voltage used to drive the motor, where the function switches with the signal from IR (Infra-Red) proximity sensor.

$$V(t) = \begin{cases} V_0 + (V_{\max} - V_0)\,\frac{t}{T_1}, & \text{for } 0 \le t \le T_1 \\ V_{\max}, & \text{for } T_1 < t < T - T_1 \\ V_{\max} - (V_{\max} - V_0)\,\frac{t}{T}, & \text{for } T - T_1 \le t \le T \end{cases}$$

According to various studies, rehabilitation exercises can require up to 30,000 cycles over six months[34]. This led us to test three cables—monofilament nylon, nylon-braided, and steel-braided—to 100,000 cycles. We observe that nylon braided cable performs well and surpasses the required cycles, as evident from Fig. 2b. Preliminary results can be found in the article[24].

A Proberos 4-strand nylon braided cable with a diameter of 0.5 mm and a load-carrying capacity of 35 kg was chosen for the current experimental study. This cable was selected for its durability and suitability in exosuit applications. The cable serves as the actuator element in the setup, simulating the tension and forces encountered in actual elbow exosuits. The selection of the cable also considers low cost, easy availability in the market, and durability.

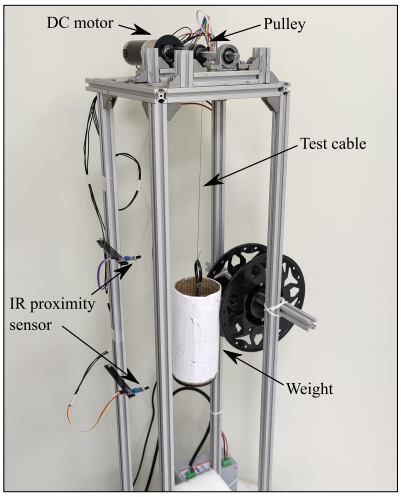

(a)

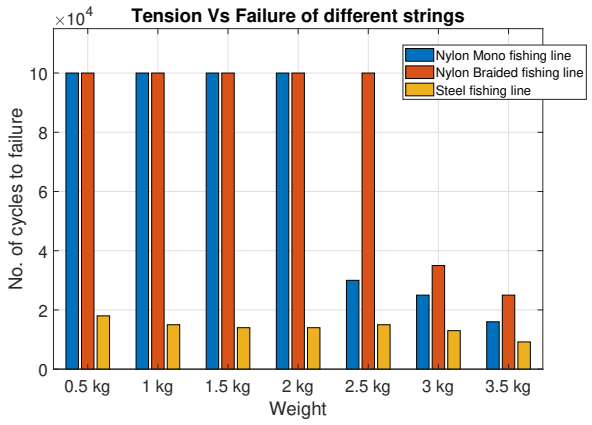

(b)

Figure 2. (a) Experimental setup to test cable under cyclic loading[24]. (b) Bar graph highlighting the number of cycles to failure for different cables under different weights.

Static model

A static model is developed for the above experimental setup, refer Fig. 1, wherein the position of the upper bar is vertical, and the lower bar flexes and extends with respect to it. The schematic of a representative position is shown in Fig. 3(I). The joint flexion is described by considering the internal angle of the joint and is denoted as 'θ'. The angle between the cable and the lower bar is 'α'. The mass of the load at the end of the lower bar in the experimental setup is denoted as 'm', while the mass of the lower bar itself is 'm_f', the mass of the load cell attachment is 'm_{lc}', and the length of the forearm bar is 'l'. The corresponding notations are highlighted in Fig. 3.

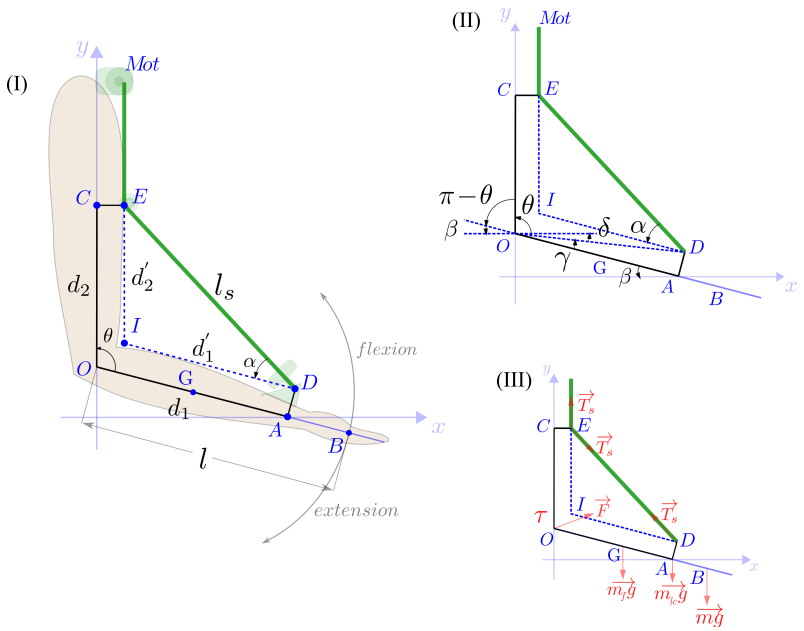

Figure 3. Schematic representation of the experimental setup. (I) highlights the geometrical parameters (II) highlights the angles. Angles are positive in an anti-clockwise direction (III) highlighting various forces on the experimental setup and moment at the elbow joint.

Let the geometric parameter be:

$$\begin{gathered} d_1 = \|OA\|,\ d_2 = \|OC\|,\ l_s = \|DE\|, \\ d_1^{'} = \|DI\|,\ d_2^{'} = \|EI\|,\ l = \|OB\| \end{gathered} \tag{1}$$

From Fig. 3(b), $\beta + \pi - \theta = \frac{\pi}{2}$.
The static equilibrium of forces and moments can be defined as in Eqns. 2 and 3

$$\vec{F} + \vec{T_s} + \overrightarrow{(m + m_f + m_{lc})g} = \vec{0} \tag{2}$$

$$\begin{gathered} \left(\overrightarrow{OD} \times \vec{T_s}\right) + \left(\overrightarrow{OB} \times \overrightarrow{mg}\right) + \left(\overrightarrow{OG} \times \overrightarrow{m_f g}\right) + \\ \left(\overrightarrow{OA} \times \overrightarrow{m_{lc} g}\right) = \vec{0} \end{gathered} \tag{3}$$

where $\vec{F}$ represents the reaction force generated at the joint under the action of cable tension, $\vec{T_s}$, and the gravity forces $\overrightarrow{m_f g}$, $\overrightarrow{m_{lc} g}$, and $\overrightarrow{mg}$. Here, g represents the acceleration due to gravity and G represents the centre of mass of the lower bar relative to the joint O.
Let T_s be the magnitude of $\vec{T_s}$. The components of the reaction force $\vec{F}$ in the x and y directions are represented in Eqn. 4.

$$\begin{gathered} F_x - T_s \cos(\alpha + \beta) = 0, \\ F_y + T_s \sin(\alpha + \beta) = (m + m_f + m_{lc})g, \end{gathered} \tag{4}$$

With $\beta = \theta - \frac{\pi}{2}$ we obtain

$$\begin{gathered} F_x - T_s \cos\left(\alpha + \theta - \frac{\pi}{2}\right) = 0, \\ F_y + T_s \sin\left(\alpha + \theta - \frac{\pi}{2}\right) = (m + m_f + m_{lc})g. \end{gathered} \tag{5}$$

The reaction forces at the joint can also be written as,

$$\begin{gathered} F_x - T_s \sin(\alpha + \theta) = 0, \\ F_y - T_s \cos(\alpha + \theta) = \left(m + m_f + m_{lc}\right) g. \end{gathered} \tag{6}$$

The anchor points on both bars and the cable between them form a triangle, as shown in Fig. 3(I). Subsequently, the triangle properties can be used to calculate the unknown variables α, γ, δ, d_1', d_2', and l_s. With the weight loaded on the experimental setup, the turning moment τ required to hold the joint at any particular joint position $\theta \in (0, \pi)$ can be formulated as shown below.

$$\tau = (mgl + m_f g\tfrac{l}{2} + m_{lc} g d_1)\sin\theta, \tag{7}$$

The Eqn. (7) determines the minimum moment to be produced by the pulling cable for the actuation of the forearm. The moment produced by the cable, τ_s, with the known distance between the actuation point and the joint can be expressed as shown in Eqn. 8

$$\tau_s = T_s \|OD\| \sin(\alpha + \gamma)\,. \tag{8}$$

where $\gamma = \tan^{-1}\left(\frac{\|AD\|}{d_1}\right)$ and $\|OD\| = \frac{d_1}{\cos(\gamma)}$,

To maintain a static equilibrium, τ and τ_s should be equal. Now, upon equating Eqn. (7) and Eqn. (8), we get

$$T_s = \frac{(mgl + m_f g\frac{l}{2} + m_{lc} g d_1)\sin\theta}{\|OD\| \sin(\alpha + \gamma)}. \tag{9}$$

With $\theta - \frac{\pi}{2} = \delta + \gamma$, coordinates of points D and E can be written as in Eqn. 10,

$$\begin{gathered} D_x = \|OD\| \sin(\gamma - \theta) \\ E_x = -\|CE\| \cos(\gamma - \theta) \\ E_y = d_2 \end{gathered} \tag{10}$$

Let I be the intersection of lines $\overline{EI}$ and $\overline{DI}$, refer Fig. 3, the coordinates I_x and I_y can be defined as in Eqn. 11, where, $a = -\cot(\theta)$ represents the slope and $c = D_y - aD_x$.

$$\begin{aligned} I_x &= E_x \\ I_y &= aE_x + c \end{aligned} \tag{11}$$

The value of α can be obtained as follows, from Fig. 3(a), using the sine equality

$$\frac{l_s}{\sin\theta} = \frac{d_2^{'}}{\sin\alpha}. \tag{12}$$

From distances $d_1^{'}$ and $d_2^{'}$, the length of the cable l_s can be calculated,

$$l_s = \sqrt{{d_1^{'}}^2 + {d_2^{'}}^2 - 2d_1^{'}d_2^{'}\cos\theta}. \tag{13}$$

Using Eqns. 12 and 13, the relation between θ and α is represented as in Eqn. 14, which is true where the inverse sine function is monotonous.

$$\alpha = \sin^{-1}\left(\frac{d_2^{'}\sin\theta}{\sqrt{{d_1^{'}}^2 + {d_2^{'}}^2 - 2d_1^{'}d_2^{'}\cos\theta}}\right) \tag{14}$$

Using the cable tension T_s, the moments in the anchor points A and C can be evaluated using Eqn. 15, where $\overrightarrow{EMot}$ represents the direction of point E to motor location Mot. Segments AD and CE are the height of the anchor points on the lower bar and upper bar respectively.

$$\begin{aligned} M_A &= \overrightarrow{AD} \times \left(\frac{\overrightarrow{DE}}{\|DE\|}\right) T_s \\ M_C &= \overrightarrow{CE} \times \left(\frac{\overrightarrow{EMot}}{\|EMot\|} + \frac{\overrightarrow{ED}}{\|ED\|}\right) T_s \end{aligned} \tag{15}$$

Although the Eqn. 14 can take values of joint angle from for $\theta \in]0, \pi[$, the actual range of motion of a human arm is different. From the anthropometric data, the range of motion of elbow joint (in terms of θ) is between 52° to 180°[32]. From the Eqn. (9) the tension in the cable, T_s, for different weights attached to the lower bar in the experimental setup can be calculated. Additionally, from the Eqn. (13) the length of the cable to be actuated, l_s, by the motor for any given joint angle 'θ' can be calculated. The tension in the cable calculated by the static model for a load at a certain joint position can be experimentally validated.

Results

The variation of cable tension, $\overrightarrow{T_s}$, reaction force at the joint, $\overrightarrow{F}$, and the perceived moment at anchor points, $\overrightarrow{M_A}$ and $\overrightarrow{M_C}$, with respect to changes in the d_1 and d_2 are presented as surface plots in Figs. 4 to 7. These plots are generated using the Eqns. 9, 6, and 15, presented in section Static model. Notably, d_1 and d_2 are varied from 0.05 to 0.15 m, with two choices of joint angles, 90° and 120°, and three choices of mass, m, 0.5 kg, 1 kg, and 2 kg, considered while generating these surface plots. From the anthropometric data,[32], the length of the upper arm and lower arm for an adult is between 0.27 m to 0.30 m. Considering the width of the arm, the closest position possible to attach an anchor point is 0.05 m from the elbow. Although the farthest position can be at the end of the arm, we have chosen a mid-way position of 0.15 m. Hence, the choice of the bounds of d_1 and d_2 are selected as 0.05 m and 0.15 m. Jeffrey et al.[35], showed that during the range of motion exercises in rehabilitation, the initial range of the exercises was limited to avoid extreme flexion or extension positions typically in the range of $80° \leq \theta \leq 120°$. For the current experiment, 90° becomes the first point of interest as forces due to gravity are maximum and 120° becomes the second point of interest being the upper bound. Also, from the anthropometric data[32], the mass of the forearm for an adult (90 percentile) is about 2 kg. Since, for most of the population, the weight of the forearm is less than 2 kg, the efforts in the experiment were studied at 0.5 kg, 1 kg, and 2 kg.

The experiment is conducted at 90° and 120°, refer Fig. 1, with the load of 0.5, 1 and 2 kg at various anchor positions, i.e., d_1 and $d_2 \in [0.05, 0.15]$. The values of tension in the cable are recorded from the load cell display. The experimental values of the distances, $AD = 0.01$ m, $CE = 0.015$ m, and masses $m_f = 0.135$ kg, and $m_{lc} = 0.015$ kg. The experimentally measured cable tension values, $T_{s_{exp}}$, and the simulated cable tension values, $T_{s_{sim}}$, calculated using the static model are compared and the corresponding % deviations are presented in Table 1. Evidently, both $T_{s_{exp}}$ and $T_{s_{sim}}$ are in close agreement.

Figure 4 shows the surface plot of the magnitude of the cable tension, T_s, with anchor point positions, d_1 and d_2. Fig. 4(a) represents the tension plot at the joint position, θ = 90°, and load of 0.5 kg. The tension in the cable, T_s, is observed to be less when the anchor points d_1 and d_2 are 0.15 m from the joint. This is because 0.15 m is the farthest position where the desired moment to hold the joint position can be generated with minimal cable tension. Furthermore, the plots Figs. 4(b) and (c) are in the same joint position, θ = 90°, but with an increased load of 1 kg and 2 kg, respectively. Noting that the tension value is proportional to the mass, refer to Eqn. 9, we observe an increase in cable tension values in Figs. 4(b) and (c). Figure 4(d) shows the tension plot at joint position, θ = 120° and load of 0.5 kg. In particular, at θ = 120°, the surface plot follows a similar trend but with minor variations in tension values compared to the surface plot at 90°. This is because the cable tension is the function of sine, refer to Eqn. 9, in both 90° and 120° positions, we observe the corresponding variation in simulated and experimental tension values, refer to Table 1, as well as surface plots. Hence, for the range of flexion or extension between $80° \leq \theta \leq 120°$ the effect of joint position is minimal. Furthermore, the plots in Figs. 4(e) and (f) are with a load of 1 kg and 2 kg at θ = 120° reported an increase in the cable tension value due to the increase in mass. The discrete points shown in blue on the surface plots are the experimental cable tension values.

Figure 5 shows the surface plot of the magnitude of the reaction force at the joint, F, with anchor point positions, d_1 and d_2. Fig. 5(a) represents the surface plot of the reaction force at the joint for the joint position, θ = 90° and load of 0.5 kg. The reaction force at the joint is calculated using the known cable tension values with Eqn. 6. As F_x and F_y are

Table 1. Comparison of simulated tension, $T_{s_{sim}}$, and experimental tension, $T_{s_{exp}}$, values and deviation for joint angles $90°$ and $120°$, with mass 0.5 kg, 1 kg, and 2 kg, with variation in anchor positions d_1 and d_2, relative to joint.

w.r.t joint		m = **0.5 kg,** $\theta = 90°$			m = **1 kg,** $\theta = 90°$			m = **2 kg,** $\theta = 90°$		
d_1	d_2	$T_{s_{sim}}$	$T_{s_{exp}}$	**Deviation**	$T_{s_{sim}}$	$T_{s_{exp}}$	**Deviation**	$T_{s_{sim}}$	$T_{s_{exp}}$	**Deviation**
0.05	0.05	37.94	40.22	6.01%	71.22	77.01	8.13%	137.79	148.33	7.69%
0.05	0.10	33.40	34.14	2.35%	62.70	61.99	1.09%	121.30	123.61	1.94%
0.05	0.15	32.94	31.59	4.17%	61.83	62.88	1.75%	119.61	118.51	0.92%
0.10	0.05	32.63	33.35	2.10%	61.14	63.59	4.01%	118.14	124.59	5.48%
0.10	0.10	21.18	20.99	0.93%	39.67	40.22	1.49%	76.66	78.28	2.18%
0.10	0.15	18.58	17.85	3.70%	34.81	34.53	0.56%	67.27	68.87	2.33%
0.15	0.05	32.42	32.77	1.21%	60.61	62.10	2.43%	116.98	116.54	0.34%
0.15	0.10	18.49	17.85	3.19%	34.57	34.14	1.14%	66.72	68.08	2.06%
0.15	0.15	14.73	15.01	2.00%	27.53	26.98	2.14%	53.14	54.25	2.03%
w.r.t joint		m = **0.5 kg,** $\theta = 120°$			m = **1 kg,** $\theta = 120°$			m = **2 kg,** $\theta = 120°$		
d_1	d_2	$T_{s_{sim}}$	$T_{s_{exp}}$	**Deviation**	$T_{s_{sim}}$	$T_{s_{exp}}$	**Deviation**	$T_{s_{sim}}$	$T_{s_{exp}}$	**Deviation**
0.05	0.05	40.54	42.58	5.03%	76.10	80.74	6.09%	147.22	152.74	3.75%
0.05	0.10	34.64	32.77	5.40%	65.02	61.31	5.70%	125.80	117.33	6.73%
0.05	0.15	32.90	32.57	1.00%	61.76	59.84	3.11%	119.49	115.66	3.20%
0.10	0.05	33.45	36.40	8.81%	62.66	62.12	5.52%	121.09	129.98	7.34%
0.10	0.10	23.98	23.64	1.42%	44.93	43.36	3.49%	86.83	83.29	4.07%
0.10	0.15	20.94	20.80	0.66%	39.23	39.93	1.78%	75.81	73.58	2.94%
0.15	0.05	31.63	35.71	12.89%	59.14	66.02	11.63%	114.15	122.04	6.91%
0.15	0.10	20.75	20.40	1.68%	38.78	38.85	0.18%	74.86	72.99	2.49%
0.15	0.15	17.07	16.97	0.58%	31.92	31.00	2.88%	61.61	60.43	1.91%

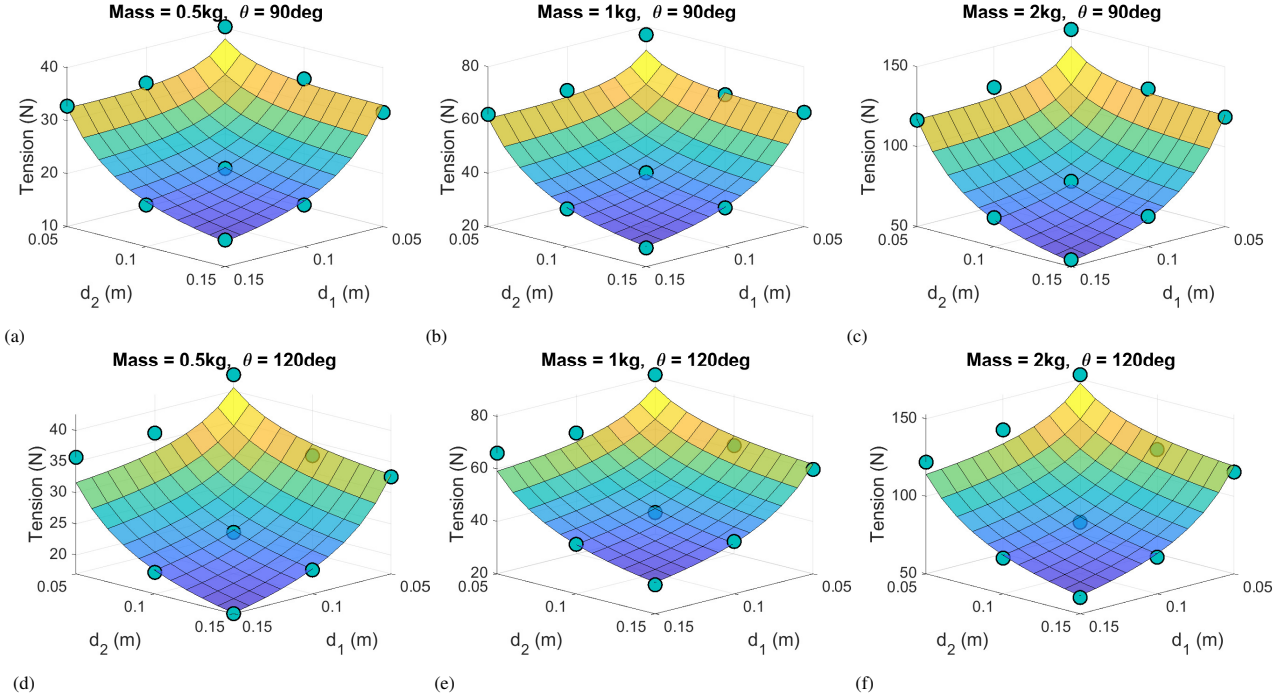

Figure 4. (a) - (f) Surface plots of simulated tension, $T_{s_{sim}}$, with variation of anchor position d_1 and d_2, at joint positions $90°$ and $120°$ and masses 0.5 kg, 1 kg and 2 kg. Discrete dots along the surface plot represent the experimentally recorded tension, $T_{s_{exp}}$ values.

proportional to the cable tension, refer Eqn. 6, and the surface plot of reaction force, Fig. 5, has a similar gradient as the surface plot of the cable tension, refer Fig. 4. Figures. 5(b) and (c) show the surface plots of the reaction force at the joint at $\theta = 90°$ for a load of 1 kg, and 2 kg respectively. The value of reaction force increased with an increase in the load. Figure. 5(d) - (f), are the surface plots of the reaction force at the joint for the joint position, $\theta = 120°$ with loads of 0.5 kg, 1 kg and 2 kg respectively. The surface plots at $120°$ exhibit the same trend as surface plots at $90°$.

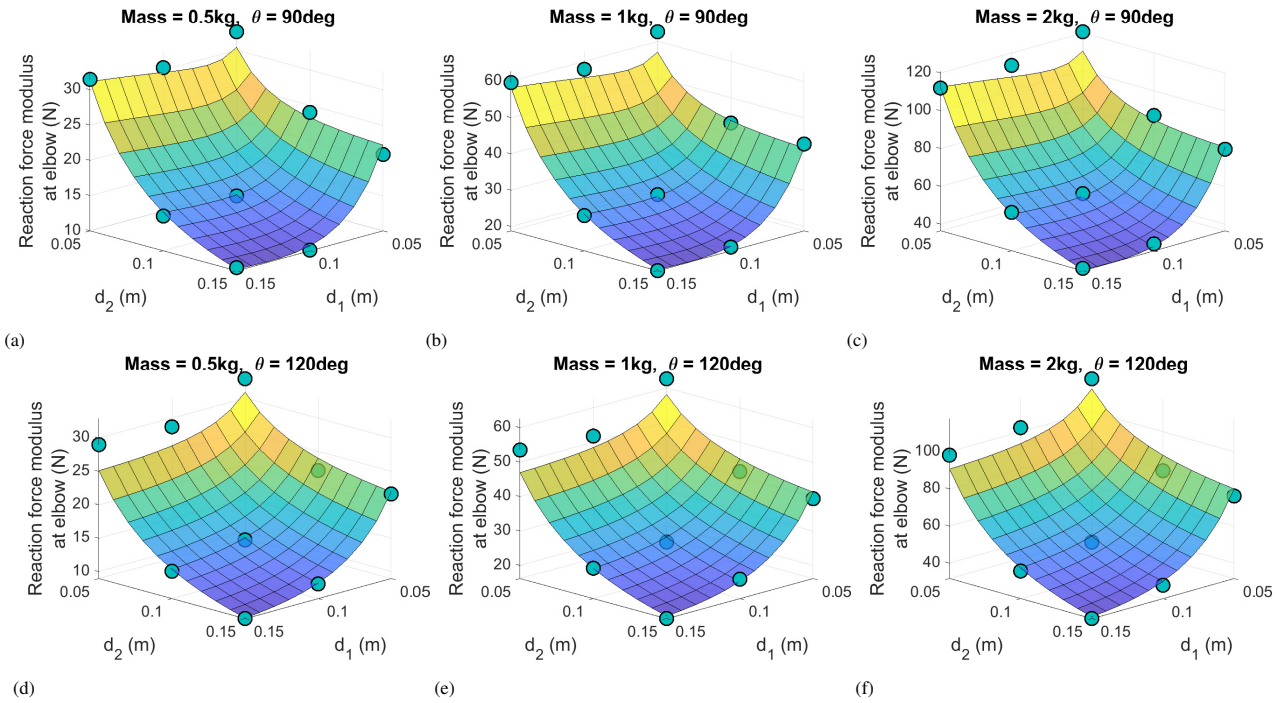

Figure 5. (a) - (f) Surface plots of the simulated reaction force at the elbow, with the variation of anchor position d_1 and d_2, at joint positions $90°$ and $120°$ and masses 0.5 kg, 1 kg, and 2 kg. Discrete dots along the surface plot represent the reaction force calculated using the experimentally recorded tension.

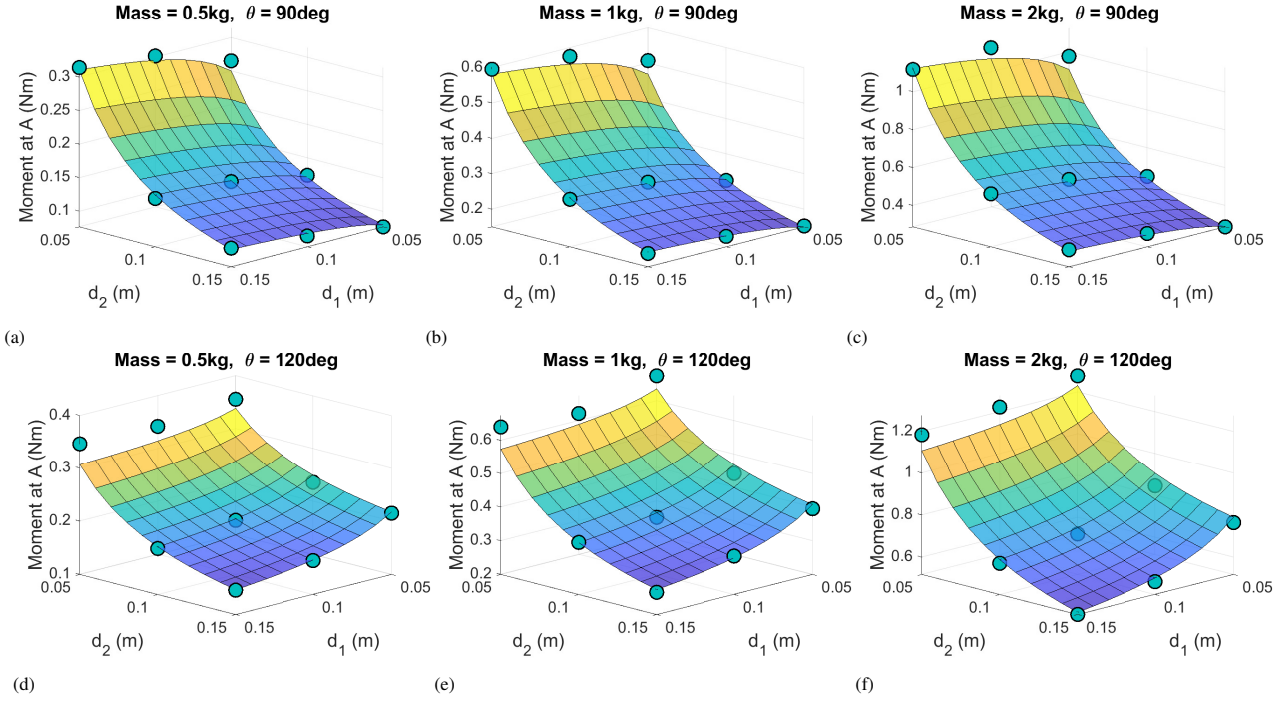

Figure 6. (a) - (f) Surface plots of the simulated moment at the anchor position A, by varying d_1 and d_2, at joint positions $90°$ and $120°$ and masses 0.5 kg, 1 kg, and 2 kg. Discrete dots along the surface plot represent the moment at A calculated using the experimentally recorded tension.

Figure 6 shows the surface plot of the moment generated, M_A, at the anchor point attachment A on the lower bar, refer Fig. 3, with anchor point positions, d_1 and d_2. Figure 6(a) is the surface plot of the moment at the anchor point attachment A, M_A, at the joint position, $\theta = 90°$ and a load of 0.5 kg. It is observed that M_A is decreasing along d_2 and remains nearly similar along d_1. From Eqn. 15, M_A depends on cable tension T_s and the attachment point A. For the case of $d_2 = 0.05$ m, the direction of $\overrightarrow{DE}$ is nearly parallel to the lower bar and nearly perpendicular to AD, for any value of d_1, refer Fig. 3, thus maximum moment is observed at this configuration. Now, $\overrightarrow{DE}$ becomes steeper when d_2 is moved from 0.05 m towards 0.15 m, for any d_1, resulting in decreasing moment. Figs. 6(b) and (c) are the plots of the moment, $\overrightarrow{M_A}$, at $\theta = 90°$ and loads of 1 kg and 2 kg. With the increase in mass, T_S increases but the configuration will

remain similar, thus we observe an increase in M_A with a similar gradient. Figure. 6(d) is surface plot for M_A at θ = 120° for a load of 0.5 kg. Unlike Fig. 6(a), we observed a change in gradient along d_1 also. The reason is, that the $\overrightarrow{DE}$ is always steeper for all possible d_2 as compared with the case of θ = 90°. Figures. 6(e) and (f) are the surface plots of M_A, at θ = 120° and load of 1 kg and 2 kg respectively. We observe a similar behaviour in gradient as reported in Fig. 6(d).

Figure 7 shows the surface plot of the moment generated, M_C, at the anchor point attachment C, refer Fig. 3, with anchor point positions, d_1 and d_2. Fig. 7(a) is the surface plot of M_C, at θ = 90° for a load of 0.5 kg. It is observed that M_C is decreasing with an increase in d_2 and increasing with an increase in d_1. From Eqn. 15, M_C depends on cable tension T_s which acts on either side of the anchor attachment E, refer Fig. 3, and the attachment point C. When d_2 is at the farthest position, and d_1 is closest to the joint, M_C is minimal because of the reduction in cable tension, T_s, along $\overrightarrow{EMot}$ and $\overrightarrow{ED}$ as the cable is nearly parallel to the upper bar, and resultant tension decreases. Conversely, if d_2 is at the closest to the joint and d_1 is farthest, then the cable tension, T_s, is higher compared to the previous case, because of an increase in resultant tension. Figs. 7(b) and (c) are the plots of the moment, $\overrightarrow{M_C}$, at θ = 90° and loads of 1 kg and 2 kg. With the increase in mass, T_S increases, thus we observe an increase in M_C with a similar gradient. Figure. 7(d) is surface plot for M_C at θ = 120° for a load of 0.5 kg. The resultant tension will reduce further with an increase in joint angle 120°, thus M_C decreases. Similar observations are reported in Figs. 7(e) and (f) for a load of 1 kg and 2 kg respectively.

With the results, the physical variables measured with the experimental setup are validated using a static model. Thus, the equations of cable tension, joint reaction forces and moments can be used to optimize the anchor point position.

Optimization of anchor positions

The surface plots (Figs. 4 to 7) suggest that the variables studied are not constant but have a gradient, with the variation of anchor positions. From numerical results and experimental measurements of cable tension we observe that the functions, $\overrightarrow{T_s}$, $\overrightarrow{F}$, $\overrightarrow{M_A}$, and $\overrightarrow{M_C}$, are convex within the studied range of anchor point positions. Hence they have a unique minimum value, which is evident from the plots, Figs. 4 to 7 . It is possible to define a minimization problem to realize optimal anchor positions. From the results of the simulation, shown in Figs. 4 to 7, it can be observed that the minimum value for each of the variables, $\overrightarrow{T_s}$, $\overrightarrow{F}$, $\overrightarrow{M_A}$, and $\overrightarrow{M_C}$, is at different anchor positions. To find the optimal anchor point positions, two cases were considered.

Case 1: Performance of the exosuit

In a cable-driven exosuit the anchor positions are typically embedded on a fabric-based structure worn by the user. Thus, the moments generated at the anchor positions essentially result in wear and tear of the fabric. Further, it causes deflections in anchor positions, leading to unbalanced forces during actuation. Therefore, it is crucial to minimize the resulting moments to improve the performance of the exosuit. So, we defined a minimization problem to reduce moments M_A and M_C, with respect to anchor positions d_1 and d_2 as presented in Eqn. 16. It should be noted that the function of the exosuit is also affected by the wear and tear of cable along with anchor point attachments [36,37]. From the results presented in Fig.2b, the chosen cable is a Nylon braided cable, which has a longer lifespan among the tested cables. Hence, the failure of anchor point attachments alone is the considered parameter for studying the performance of the device. For optimization, at each joint position, using a gradient descent algorithm the optimal d_1 and d_2 are identified between the bounds of 0.05 m to 0.15 m. Although, for a typical rehabilitation paradigm, the elbow range of motion varies from 80° to 120°, the optimization is done for full range of motion of a healthy individual, i.e., between 52° to 180° [32].

$$\min \left(\left\| \overrightarrow{M_A} \right\| + \left\| \overrightarrow{M_C} \right\| \right) \Big|_{(d_1,d_2)} \tag{16}$$

Figure. 8a shows the optimum positions of d_1 and d_2 for the chosen joint range of motion. It is observed that d_2 is converging towards the upper bound, implying the farthest position on the upper arm from the elbow joint for the complete range of motion. Additionally, d_1 varies within the bounds. To comprehend the behaviour of d_1 we presented three schematics, refer Fig. 8b, which represents three different joint positions 55°, 90°, and 120°. The green colour cable in each schematic represents the optimal position of d_1 on the forearm, while the red colour cable represents non-optimal positions. From Fig. 8b(I), at the optimal position, the cable and anchor point are aligned, resulting in a minimal moment at A, which is not the case for the other two positions. At a 90° joint position, as shown in Fig. 8b(II), at the optimal position, the cable becomes steeper when d_1 is closest to the elbow, and hence, generates a lesser moment at anchor position A, which is not the case for the other two positions. Further, at 120°, as shown in Fig. 8b(III), at optimal position d_1 which is farthest from the elbow, resulting in the minimum moment at A as cable tension is lowest, refer Eqn. 9. This optimization was performed with a 0.5 kg load, and the trend remains consistent for other loads.

Case 2: Comfort to the wearer

In a cable-driven exosuit, the user experiences the pull generated by the cable and the reaction forces generated at the elbow joint because of the cable pull. To enhance the wearer's comfort, both the cable tension, $\overrightarrow{T_s}$, and the reaction force, $\overrightarrow{F}$, at the elbow should be minimized. The pressure exerted on the wearer's skin during actuation is another parameter to assess comfort. However, the pressure experienced is proportional to the tension, and minimizing tension implicitly minimizes the pressure. Moreover, the pressure generated by the tension values presented in this work is within the pain pressure tolerance limit [26]. Therefore, we defined a minimization problem to reduce $\overrightarrow{T_s}$ and $\overrightarrow{F}$ with respect to the anchor positions d_1 and d_2, as presented in Eqn. 17. The bounds and range of motion for the

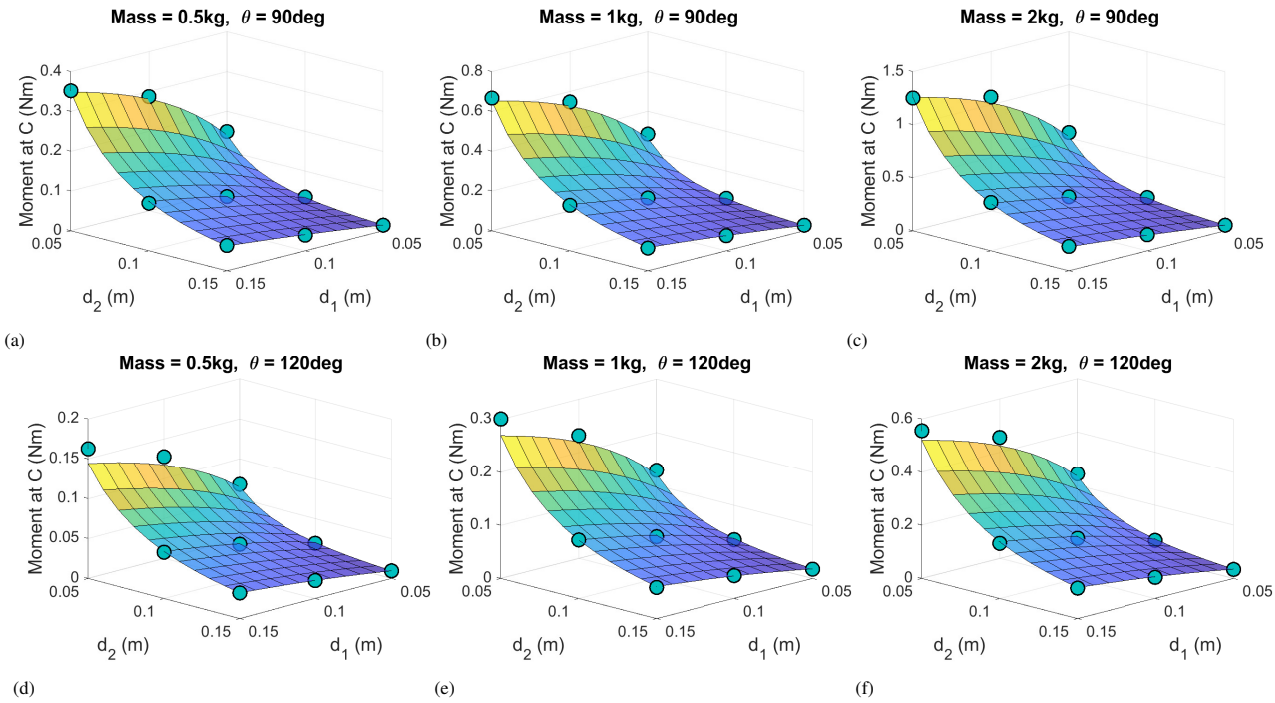

Figure 7. (a) - (f) Surface plots of the simulated moment at the anchor position C, by varying d_1 and d_2, at joint positions $90°$ and $120°$ and masses 0.5 kg, 1 kg, and 2 kg. Discrete dots along the surface plot represent the moment at C calculated using the experimentally recorded tension.

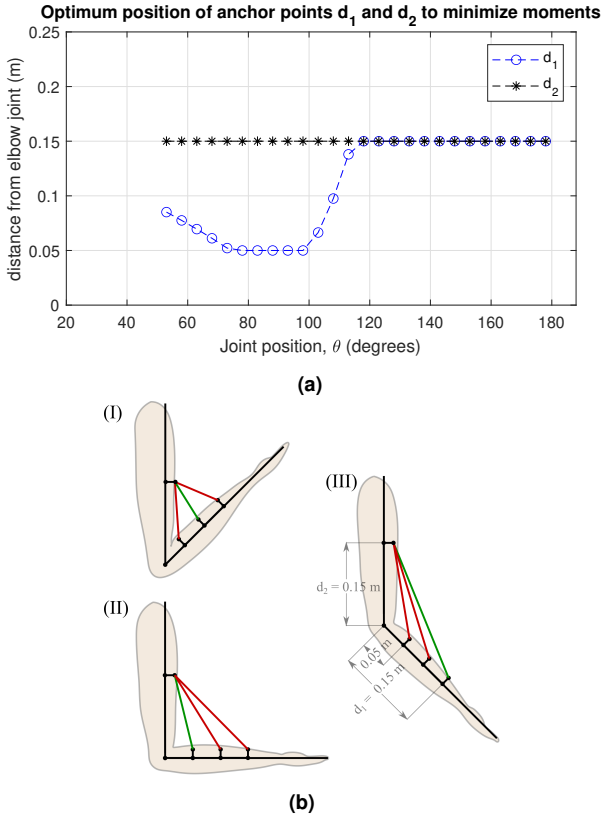

Figure 8. (a) Variation of optimal anchor positions, d_1 and d_2, along the elbow joint angle, to minimize the moment generated at anchor positions. (b) I, II and III depict the scenario of cable attached at different values of d_1 and d_2 for joint positions $55°$, $90°$, and $120°$. Green and Red cables represent optimal and non-optimal positions.

optimization are the same as discussed in Case 1.

$$\min \left(\left\| \vec{T_s} \right\| + \left\| \vec{F} \right\| \right) \Big|_{(d_1,d_2)} \tag{17}$$

Figure 9a shows that the optimal positions of d_2, converges towards the upper bound. Similarly, d_1 also converges mostly towards the upper bound excluding the extreme joint angles. To comprehend the results, we presented three schematics, refer to Fig. 9b, which represent three different joint positions $55°$, $90°$, and $120°$. The green colour cable in each of these schematics represents the optimal position and the red colour represents the non-optimal position of d_1 on the forearm. Fig. 9b(I), the angle made by the cable, is in line with the anchor attachment. Thus the tension in the cable is less, and consequently, the joint reaction force is also less. Figures. 9b(II) and 9b(III), the attachment of the anchor on the forearm at the farthest position from the elbow leads to minimal tension in the cable and the reaction force. The above optimization is performed at a load of 0.5 kg, and the trend remains consistent for other loads.

Discussion

The range of motion exercises performed during rehabilitation target to achieve the functionality of activities of daily living (ADL). These repetitive tasks are usually performed one after the other and are distinguishable in the workspace above and below $90°$. For instance, for multiple subjects, the elbow joint position was mostly under $90°$, during rehabilitation sessions with Armeo® Spring[35]. For the elbow, to restore motion after an olecranon fracture, the active flexion exercises are restricted from $80°$ to full extension initially[34]. In the case of a coronoid fracture, the extension is restricted between $120°$ to $140°$ for the rehabilitation[34]. Also,

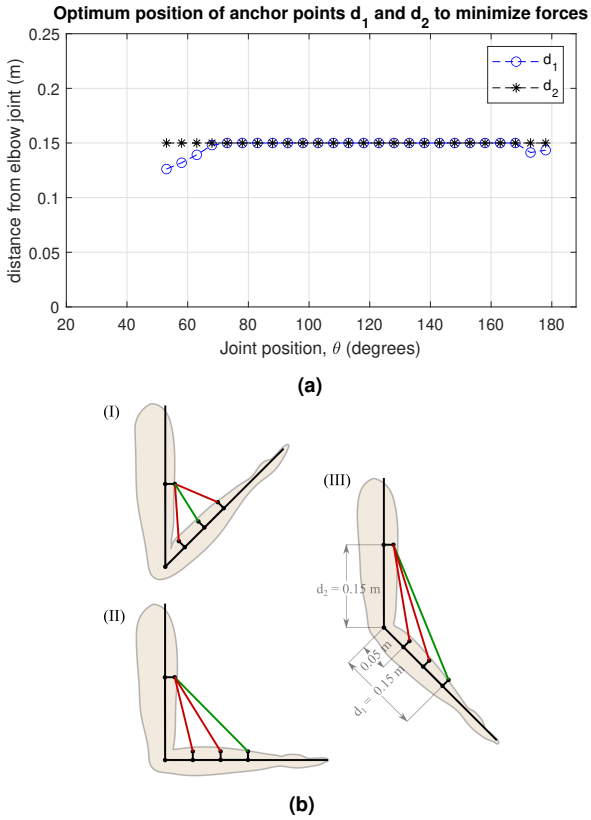

Figure 9. (a) Variation of optimal anchor positions, d_1 and d_2, with respect to the elbow joint angle, to minimize cable tension and reaction force at the elbow joint. (b) I, II and III depict the scenario of cable attached at different values of d_1 and d_2 for joint positions $55°$, $90°$, and $120°$. Green and Red cable represents optimal and non-optimal position.

all these rehabilitation exercises are repeated around 15 to 20 times per hour, which makes understanding cable-driven exosuit performance critical[34]. If a cable-driven exosuit is used for assistance during rehabilitation, the optimal position of anchor points can be chosen depending on the workspace of the intended task[13,14].

From the presented results, if our aim is to optimize the performance of the cable-driven exosuit, then for the range of motion of exercise within $100°$, anchor point d_1 can be attached closer to the elbow, and for exercises beyond $100°$, both anchor points d_1 and d_2 can be placed farthest from the elbow. Further, if our aim is to optimize the comfort then the results suggest that both the anchor positions d_1 and d_2 should be farthest from the joint. These two scenarios depend on the time of the operation. For example, if the device is used on multiple subjects for short durations, the performance of the device can be prioritized over user comfort. If the device is used on a single subject over a longer duration, the comfort of the wearer should be prioritized.

Current state-of-the-art studies on cable-driven elbow exoskeletons optimize the position of anchor points around the upper arm and forearm while keeping the distance from the elbow fixed[29,30]. However, from the above results, it is evident that there is a significant change in the cable tension with the position of the anchor points from the elbow, along the joint position. Figure 8a shows that the effective position varies by a significant margin for a good performance of the device. The position of the anchor point from the elbow is hence an important optimization parameter along with the anchor position around the axis of the arm.

The design of an exoskeleton to reduce reaction forces at joints due to misalignments in wearable devices has been presented in a study[38]. In another paper, the reaction forces at joints during the interaction of wearable devices with digital human models have been reviewed[39]. Studying the physical load on the wearer's body is important for designing a comfortable wearable device. The presented results study the change in reaction force at the elbow due to the anchor position from the elbow joint. This will aid in understanding the magnitude of reaction forces for different anchor positions from the elbow joint. This can further be incorporated into the design of the cable-driven elbow exosuit.

Several studies suggest that during the rehabilitation period, longer durations of training on rehabilitation robots will have improved results and faster recovery[40–42]. For cable-driven wearable devices, the wear and tear of anchor point attachments becomes an important parameter to be studied to have a better performance, for a longer duration of operation[36,37]. The presented results suggest that the anchor point position from the elbow will affect wear and tear at the anchor point attachment. Considering these changes in the position of anchor point placement the moments generated at anchor point attachment are reduced, which will reduce the wear and tear.

The static model also calculates the tension in the cable, $\overrightarrow{T_s}$, refer Eqn. 9, and the length of the cable between the anchor points at all the joint positions, l_s, refer Eqn. 13. These two variables can be further used to develop a control system for a cable-driven elbow exosuit. The presented results can be used for a cable-driven rehabilitation device for elbow actuation. However, one limitation is while assisting a healthy subject with daily activities, the actuation is faster and a dynamic model should be considered. To focus exclusively on the significance of the position of the anchor point from the elbow, this study does not consider the cable routing around the arm. In a future study, along with the distance from the anchor point, cable routing optimization will be considered. Also, for a future study, the comfort of the wearer can be studied by considering the pressure experienced by the user while wearing an exosuit device fabricated using these considerations.

Conclusion

This study presents a comprehensive analysis of a cable-driven experiment setup mimicking exosuit for elbow joint actuation. By developing a static model and conducting experiments, we have successfully quantified the impact of anchor point positions on cable tension, reaction forces and moments. There is a coherence between the experimental results and the estimations obtained from the static model. The results demonstrate that optimizing anchor point placement is crucial for enhancing exosuit performance and wearer comfort. The findings offer valuable guidelines for designing future cable-driven exosuits tailored to specific

rehabilitation needs. In the future, we intend to incorporate these optimized anchor positions in a cable-driven exosuit and assess the performance of the device and user comfort, by conducting experiments on healthy human subjects.

Acknowledgements

We would like to thank Mahindra University, Hyderabad, India, for the infrastructure and support. We would also like to thank Centrale Nantes, Nantes, France for aiding this work through a cotutelle with Mahindra University. And, we would also like to thank Mr. Siddharth Patil for his help collecting experimental data.

Declaration of conflicting interests

The authors declare that there are no conflicts of interest.

Funding

This research is supported by funding from the I-Hub Foundation for Robotics (IHFC), New Delhi, India (Grant No. - GP/2021/RR/017). Centrale Nantes, France, also financially supports this work.

References

1. Xiong H and Diao X. A review of cable-driven rehabilitation devices. Disability and Rehabilitation: Assistive Technology 2020; 15(8): 885–897.
2. De Iaco L, Veerbeek JM, Ket JC et al. Upper limb robots for recovery of motor arm function in patients with stroke: A systematic review and meta-analysis. Neurology 2024; 103(2): e209495.
3. Randazzo L, Iturrate I, Perdikis S et al. mano: A wearable hand exoskeleton for activities of daily living and neurorehabilitation. IEEE Robotics and Automation Letters 2017; 3(1): 500–507.
4. Zimmermann Y, Forino A, Riener R et al. Anyexo: a versatile and dynamic upper-limb rehabilitation robot. IEEE Robotics and Automation Letters 2019; 4(4): 3649–3656.
5. Lessard S, Pansodtee P, Robbins A et al. Crux: A compliant robotic upper-extremity exosuit for lightweight, portable, multi-joint muscular augmentation. In 2017 International Conference on Rehabilitation Robotics (ICORR). IEEE, pp. 1633–1638.
6. Fareh R, Elsabe A, Baziyad M et al. Will your next therapist be a robot?—a review of the advancements in robotic upper extremity rehabilitation. Sensors 2023; 23(11): 5054.
7. Balasubramanian S, Wei R, Perez M et al. Rupert: An exoskeleton robot for assisting rehabilitation of arm functions. In 2008 virtual rehabilitation. IEEE, pp. 163–167.
8. Iyer SS, Joseph JV, Sanjeevi N et al. Development and applicability of a cable-driven wearable adaptive rehabilitation suit (wears). In 2019 28th IEEE International Conference on Robot and Human Interactive Communication (RO-MAN). IEEE, pp. 1–6.
9. Chen T, Casas R and Lum PS. An elbow exoskeleton for upper limb rehabilitation with series elastic actuator and cable-driven differential. IEEE Transactions on Robotics 2019; 35(6): 1464–1474. DOI:10.1109/TRO.2019.2930915.
10. Bardi E, Gandolla M, Braghin F et al. Upper limb soft robotic wearable devices: a systematic review. Journal of NeuroEngineering and Rehabilitation 2022; 19(1): 1–17.
11. Sanjuan J, Castillo AD, Padilla MA et al. Cable driven exoskeleton for upper-limb rehabilitation: A design review. Robotics and Autonomous Systems 2020; 126: 103445.
12. Pyeon D, Ahn J, Kim DH et al. A cable-driven exosuit for bidirectional upper limb resistance exercises. IEEE Robotics and Automation Letters 2024; : 1–8DOI:10.1109/LRA.2024.3455947.
13. Javier Bermejo-García FRS Daniel Rodríguez Jorge and Alonso FJ. Dynamic optimization of anchor points positions in a cable driven exosuit: a computer simulation approach. Mechanics Based Design of Structures and Machines 2024; 52(8): 5118–5132. DOI:10.1080/15397734.2023.2248247.
14. Lu Y, Aoustin Y and Arakelian V. Optimization of design parameters and improvement of human comfort conditions in an upper-limb exosuit for assistance. Multibody System Dynamics 2024; DOI:10.1007/s11044-024-09977-1.
15. Shi Y, Gao Y, Lin W et al. A cable-driven exosuit for upper limbs: design, control, and evaluation. Proceedings of the Institution of Mechanical Engineers, Part C: Journal of Mechanical Engineering Science 2024; 0(0). DOI:10.1177/09544062241258909.
16. Harbauer C, Fleischer M, Nguyen T et al. Too close to comfort? a new approach of designing a soft cable-driven exoskeleton for lifting tasks under ergonomic aspects. In 2020 3rd International Conference on Intelligent Robotic and Control Engineering (IRCE). pp. 105–109.
17. Miranda A, Yasutomi A, Souit C et al. Bioinspired mechanical design of an upper limb exoskeleton for rehabilitation and motor control assessment. In 2012 4th IEEE RAS & EMBS International Conference on Biomedical Robotics and Biomechatronics (BioRob). pp. 1776–1781.
18. Laribi M and Ceccarelli M. Design and experimental characterization of a cable-driven elbow assisting device. Journal of Medical Devices 2021; 15(1): 014503.
19. John I, Mohan S and Wenger P. Kinetostatic analysis of a spatial cable-actuated variable stiffness joint. Journal Of Mechanisms And Robotics 2023; : 1–21.
20. Furet M and Wenger P. Kinetostatic analysis and actuation strategy of a planar tensegrity 2-x manipulator. Journal of Mechanisms and Robotics 2019; 11(6): 060904.
21. Wang J, Wang Y, Fei Y et al. Kinetostatic analysis of pneumatic bending soft actuator coupling with revolute joint. Journal of Mechanisms and Robotics 2023; 15(6): 061013.
22. Morrey B, Askew L and Chao E. A biomechanical study of normal functional elbow motion. The Journal of Bone and Joint Surgery American Volume 1981; 63: 872–877.
23. Oosterwijk A, Nieuwenhuis M, Schans C et al. Shoulder and elbow range of motion for the performance of activities of daily living: A systematic review. Physiotherapy Theory and Practice 2018; 34: 505–528.
24. Alapati S and Seth D. Testing of different strings for their usability in actuation of exosuits. In Digital Human Modeling and Applications in Health, Safety, Ergonomics and Risk Management. Anthropometry, Human Behavior, and Communication: 13th International Conference, DHM 2022, Held as Part of the 24th HCI International Conference, HCII 2022, Virtual Event, June 26–July 1, 2022, Proceedings, Part I. pp. 3–15.
25. Kermavnar T, Power V, Eyto A et al. Cuff pressure algometry in patients with chronic pain as guidance for circumferential tissue compression for wearable soft exoskeletons: a systematic

review. Soft Robotics 2018; 5(5): 497–511.
26. Rocon E, Ruiz A, Raya R et al. Human-robot physical interaction. In Wearable Robots: Biomechatronic Exoskeletons. 2008. pp. 127–163.
27. Yandell M, Ziemnicki D, McDonald K et al. Characterizing the comfort limits of forces applied to the shoulders, thigh and shank to inform exosuit design. PloS One 2020; 15(5): e0228536.
28. Bardi E, Ambrosini E, Pirelli A et al. Upper limb exosuit cable routing optimization. In 2022 International Conference on Rehabilitation Robotics (ICORR). IEEE, pp. 1–6.
29. Mao Y and Agrawal SK. Design of a cable-driven arm exoskeleton (carex) for neural rehabilitation. IEEE transactions on robotics 2012; 28(4): 922–931.
30. Shi K, Song A and Li H. Optimized design for cable-driven shoulder-elbow exoskeleton robot. IEEE Access 2021; 9: 68197–68207.
31. Wei W, Qu Z, Wang W et al. Design on the bowden cable-driven upper limb soft exoskeleton. Applied bionics and biomechanics 2018; 2018(1): 1925694.
32. Dreyfuss H, Associates H and Tilley A. The Measure of Man and Woman: Human Factors in Design. Whitney Library of Design, 1993.
33. Goiriena A, Retolaza I, Cenitagoya A et al. Analysis of bowden cable transmission performance for orthosis applications. In 2009 IEEE International Conference on Mechatronics. pp. 1–6.
34. Chinchalkar S and Szekeres M. Rehabilitation of elbow trauma. Hand Clinics 2004; 20: 363–374.
35. Schneider J, Ozsecen M, Muraoka N et al. Feasibility of an exoskeleton-based interactive video game system for upper extremity burn contractures. PM&R 2016; 8: 445–452.
36. Nasr A, Inkol K and McPhee J. Safety in wearable robotic exoskeletons: Design, control, and testing guidelines. Journal of Mechanisms and Robotics 2025; 17(5).
37. Perez Vidal AF, Rumbo Morales JY, Ortiz Torres G et al. Soft exoskeletons: Development, requirements, and challenges of the last decade. In Actuators, volume 10. MDPI, p. 166.
38. Stienen AHA, Hekman EEG, Prange GB et al. Dampace: Design of an exoskeleton for force-coordination training in upper-extremity rehabilitation. Journal of Medical Devices 2009; 3(3): 031003.
39. Scherb D, Wartzack S and Miehling J. Modelling the interaction between wearable assistive devices and digital human models—a systematic review. Frontiers in bioengineering and biotechnology 2023; 10: 1044275.
40. Molteni F, Gasperini G, Cannaviello G et al. Exoskeleton and end-effector robots for upper and lower limbs rehabilitation: narrative review. PM&R 2018; 10(9): S174–S188.
41. Teasell R, Mehta S, Pereira S et al. Time to rethink long-term rehabilitation management of stroke patients. Topics in stroke rehabilitation 2012; 19(6): 457–462.
42. Clark B, Whitall J, Kwakkel G et al. Effect of time spent in rehabilitation on activity limitation and impairment after stroke: A cochrane review summary. Stroke 2022; 53(8): e388–e389.